Experimental investigation of micro-chaos

Gergely Gyebrószki*, Gábor Csernák**, Csaba Budai***
*Department of Applied Mechanics, Budapest University of Technology and Economics, Budapest, Hungary
**MTA-BME Research Group on Dynamics of Machines and Vehicles, Budapest, Hungary
***Department of Mechatronics, Optics and Mechanical Engineering Informatics, Budapest University of Technology and Economics, Budapest, Hungary

Summary. Micro-chaos is a phenomenon when small amplitude chaotic oscillations are inflicted by digital effects (sampling, round-off and processing delay). In previous works, various digitally controlled unstable linear mechanical systems were analysed; the corresponding micro-chaos maps were derived and the coexistence of several disconnected chaotic attractors was proven. The distance of the farthest attractor from the desired state can be quite large, while the size of these attractors is usually negligible from practical point of view. This is why the phenomenon could be the source of remarkable control error. In this paper, the micro-chaos map of the PD-controlled inverted pendulum – with rounding applied to the calculated control effort, and considering dry friction – is examined by modified Simple Cell Mapping methods and the possibility of constructing an experimental device showing the phenomenon of micro-chaos is analysed. A device having variable control force resolution is presented, and experiments are carried out to verify the theoretical and numerical results.

Introduction

While sampling and delay are commonly taken into account in control problems, rounding is usually neglected. It has been shown [1], that rounding leads to small amplitude chaotic oscillations – referred to as *micro-chaos* – where several disconnected attractors may co-exist. In some simple cases (inverted pendulum stabilized with D-control with and without delay and PD-control without delay [2]), it has been proven, that the vibrations are indeed chaotic. The chaotic behaviour highly depends on where the rounding is applied. In this paper the PD-controlled inverted pendulum – with rounding applied to the measured position, angular velocity and control torque – is analysed, while the effect of dry friction is taken into account.

PD-controlled inverted pendulum with damping and dry friction

The *pendulum-on-a-cart* is one of the simplest devices used for demonstrating control problems. Neglecting the cart part of this device leads to a simple inverted pendulum with control. In this section, the equation of motion of the digitally controlled inverted pendulum is presented and the formulation of the dimensionless map representing the solution is shown.

Solution of the equation of motion

Consider an inverted pendulum with damping, friction, and digitally implemented PD-control with zero order hold (i.e. the control torque is constant between two successive sampling instants) as shown in Figure 1. The equation of motion of

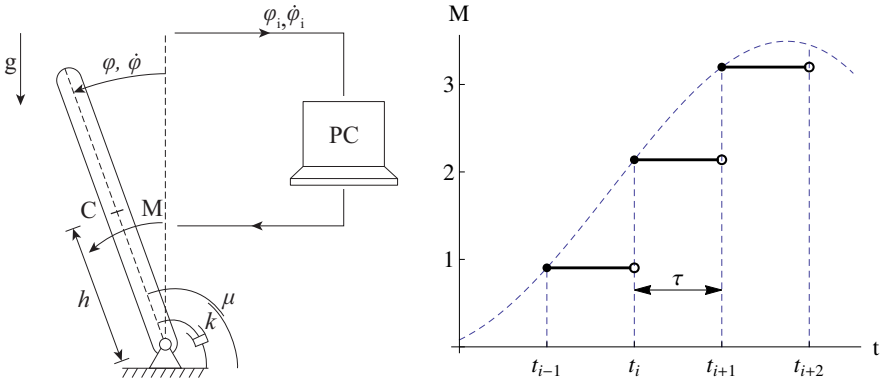

Figure 1: The digitally controlled inverted pendulum and the control torque with respect to time.

this system is

$$J\,\ddot{\varphi}(t) = mgh\sin(\varphi(t)) - k\,\dot{\varphi}(t) - p\,\varphi_i - d\,\dot{\varphi}_i - \operatorname{sgn}(\dot{\varphi}(t))\,\mu M_0, \qquad t \in [i\tau, (i+1)\tau), \tag{1}$$

where m is the mass of the pendulum, J is the mass moment of inertia about the axis of rotation, h is the distance between the centre of mass and the axis of rotation, p and d are control parameters, k is the linear damping coefficient, μM_0 is the bearing friction and μ is the coefficient of kinetic friction (considered to be equal to the coefficient of static friction), g is the gravitational acceleration, τ is the sampling time, while $\varphi_i = \varphi(i\tau)$ and $\dot{\varphi}_i = \dot{\varphi}(i\tau)$ are sampled values of the

angular position and angular velocity respectively (at the beginning of the i-th time interval). Rearranging, and linearizing (1) yields

$$\ddot{\varphi}(t) + 2\beta\dot{\varphi}(t) - \alpha^2\varphi(t) = -P\,\varphi_i - D\,\dot{\varphi}_i - \mathrm{sgn}(\dot{\varphi}(t))\,\mu_0, \tag{2}$$

where $\alpha^2 = \frac{mgh}{J}, 2\beta = \frac{k}{J}, P = \frac{p}{J}, D = \frac{d}{J}, \mu_0 = \frac{\mu M_0}{J}$.
One can rewrite (2) as a system of first order differential equations:

$$\begin{aligned} \dot{\omega}(t) &= \alpha^2\varphi(t) - 2\beta\dot{\varphi}(t) - P\,\varphi_i - D\,\omega_i - \mathrm{sgn}(\dot{\varphi}(t))\,\mu_0, \qquad t \in [i\tau, (i+1)\tau)\,, \\ \dot{\varphi}(t) &= \omega(t), \end{aligned} \tag{3}$$

with initial conditions: $\omega(i\tau) = \omega_i, \varphi(i\tau) = \varphi_i$. Without considering rounding, and using the notations $\hat{\alpha} = \alpha\tau$, $\hat{\beta} = \beta\tau$, $\hat{\gamma} = \sqrt{\hat{\alpha}^2 + \hat{\beta}^2}$, $\hat{p} = P\tau^2$, $\hat{d} = D\tau$, $x = \varphi/\varphi_{\mathrm{ref}}$,$v = \omega/\omega_{\mathrm{ref}}$, $\hat{\mu} = \mu_0\,\tau^2/\varphi_{\mathrm{ref}}$, $\mathbf{y} = \begin{bmatrix} x & v \end{bmatrix}^T$ the solution formulates a dimensionless 2D map:

$$\mathbf{y}_{i+1} = (\mathbf{U} + \mathbf{B}\,\mathbf{K})\,\mathbf{y}_i + \mathrm{sgn}(y_{i,2})\,\hat{\mu}\,\mathbf{B}, \tag{4}$$

where

$$\begin{aligned} \mathbf{U} &= \frac{e^{-\hat{\beta}}}{\hat{\gamma}} \begin{bmatrix} \hat{\gamma}\cosh(\hat{\gamma}) + \hat{\beta}\sinh(\hat{\gamma}) & \sinh(\hat{\gamma}) \\ \hat{\alpha}^2\sinh(\hat{\gamma}) & \hat{\gamma}\cosh(\hat{\gamma}) - \hat{\beta}\sinh(\hat{\gamma}) \end{bmatrix}, \\ \mathbf{B} &= \frac{e^{-\hat{\beta}}}{\hat{\gamma}} \begin{bmatrix} \frac{\hat{\gamma}\,e^{\hat{\beta}} - \hat{\gamma}\cosh(\hat{\gamma}) - \hat{\beta}\sinh(\hat{\gamma})}{\alpha^2} \\ -\sinh(\hat{\gamma}) \end{bmatrix}, \\ \mathbf{K} &= \begin{bmatrix} \hat{p} & \hat{d} \end{bmatrix}. \end{aligned}$$

Map (4) yields the solution of the system at sampling instants ($t \in \mathrm{k}\,\tau, \mathrm{k} \in \mathbb{Z}$) as long as the sign of the velocity ($\mathrm{sgn}(y_{i,2})$) does not change within the sampling interval. However the change in the sign of the velocity usually happens within sampling intervals therefore the formulation of the solution requires additional calculations.

Dealing with the friction force

The solution of (3) from a given initial condition $\mathbf{y}_i$ with respect to the dimensionless time $s \in [0, 1)$ can be written as:

$$\mathbf{y}(s) = (\mathbf{\Phi}(s) + \boldsymbol{\delta}(s)\,\mathbf{K})\,\mathbf{y}_i + \mathrm{sgn}(y_{i,2})\,\hat{\mu}\,\boldsymbol{\delta}(s), \tag{5}$$

where

$$\begin{aligned} \mathbf{\Phi}(s) &= \frac{e^{-\hat{\beta}\,s}}{\hat{\gamma}} \begin{bmatrix} \hat{\gamma}\cosh(\hat{\gamma}\,s) + \hat{\beta}\sinh(\hat{\gamma}\,s) & \sinh(\hat{\gamma}\,s) \\ \hat{\alpha}^2\sinh(\hat{\gamma}\,s) & \hat{\gamma}\cosh(\hat{\gamma}\,s) - \hat{\beta}\sinh(\hat{\gamma}\,s) \end{bmatrix}, \\ \boldsymbol{\delta}(s) &= \frac{e^{-\hat{\beta}\,s}}{\hat{\gamma}} \begin{bmatrix} \frac{\hat{\gamma}\,e^{\hat{\beta}\,s} - \hat{\gamma}\cosh(\hat{\gamma}\,s) - \hat{\beta}\sinh(\hat{\gamma}\,s)}{\alpha^2} \\ -\sinh(\hat{\gamma}\,s) \end{bmatrix}. \end{aligned}$$

To calculate the dimensionless time, when the solution reaches the switching line of the friction force (i.e. where the velocity is equal to zero), the velocity expressed from (5) is examined:

$$\frac{e^{-\hat{\beta}\,s_0}}{\hat{\gamma}} \left(\hat{\gamma}\,v_i\cosh(\hat{\gamma}\,s_0) - \left((\hat{\beta} + \hat{d})\,v_i + \left(\hat{p} - \hat{\alpha}^2\right)\,x_i + \mathrm{sgn}(v_i)\,\hat{\mu}\right)\sinh(\hat{\gamma}\,s_0)\right) = 0 \tag{6}$$

From Eq. (6) the dimensionless time corresponding to zero velocity can be expressed:

$$s_0 = \frac{1}{\hat{\gamma}}\log\left(\sqrt{\frac{S - C}{S + C}}\right), \tag{7}$$

where S and C are the coefficients of $\sinh(\hat{\gamma}\,s_0)$ and $\cosh(\hat{\gamma}\,s_0)$ respectively:

$$\begin{aligned} S &= -\left((\hat{\beta} + \hat{d})\,v_i + \left(\hat{p} - \hat{\alpha}^2\right)\,x_i + \mathrm{sgn}(v_i)\,\hat{\mu}\right), \\ C &= \hat{\gamma}\,v_i. \end{aligned}$$

The condition of crossing the switching line of the friction force within the same sampling interval:

$$0 < s_0 < 1, \tag{8}$$

and the condition of sticking:

$$\mathrm{abs}(\hat{p}\,x_i + \hat{d}\,v_i - \hat{\alpha}^2\,x(s_0)) < \hat{\mu}. \tag{9}$$

Note that the calculated control force does not change within the sampling interval (due to the zero order hold). Upon applying Map (4) one should calculate s_0 (Eq. (7)) to check whether the resulting state can be accepted. If condition (8) is true, then instead of applying Map (4), Map (5) should be applied with $s = s_0$. Afterwards the condition of sticking should be checked. If the condition evaluates to false, Map (5) should be applied again with $s = 1 - s_0$ to calculate the solution for the rest of the current sampling interval.

The micro-chaos map

This section describes the formulation of the so-called *micro-chaos map* [3] as the combination of rounding and Map (4).

Rounding at the input

If the measured position has a resolution of $r_{\text{in}}[\text{rad}]$, and the resolution of the velocity (which is assumed to be calculated from the position) is r_{in}/τ, Map (4) with the rounding can be written as:

$$\mathbf{y}_{i+1} = (\mathbf{U} + \mathbf{B}\,\mathbf{K})\,\text{Int}(\mathbf{y}_i) + \text{sgn}(\text{Int}(y_{i,2}))\,\hat{\mu}\,\mathbf{B}, \tag{10}$$

where the reference angle in $\mathbf{y}_i$ is $\varphi_{\text{ref}} = r_{\text{in}}$ and the reference angular velocity is $\omega_{\text{ref}} = r_{\text{in}}/\tau$. Equation (10) is called *micro-chaos map* or *μ-chaos map*. ($\text{Int}(n)$ denotes rounding towards zero i.e., taking the integer part of n, or shortly *truncation*.)

Rounding at the output

When rounding is applied to the calculated control effort (i.e. to the output of the control system), the following *micro-chaos map* is obtained:

$$\mathbf{y}_{i+1} = \mathbf{U}\,\mathbf{y}_i + \mathbf{B}\,(\text{Int}(\mathbf{K}\,\mathbf{y}_i) + \text{sgn}(y_{i,2})\,\hat{\mu})\,. \tag{11}$$

Here the reference angle in $\mathbf{y}$ is $\varphi_{\text{ref}} = r_{\text{out}}\tau^2$, the reference angular velocity is $\omega_{\text{ref}} = r_{\text{out}}\tau$, while $r_{\text{out}}\left[\frac{\text{rad}}{\text{s}^2}\right]$ is the resolution of the actuated control effort.

Rounding at the input and output

In the combination of the previous two cases using $\varphi_{\text{ref}} = r_{\text{out}}\tau^2$ to scale the position and introducing the dimensionless time $T = t/\tau$, while using the notation $\square' = \frac{\text{d}}{\text{d}T}\square$, Equation (2) takes the form

$$x''(T) + 2\hat{\beta}x'(T) - \hat{\alpha}^2 x(T) = -\text{Int}\left(\hat{p}\,\rho\,\text{Int}\left(\frac{x_i}{\rho}\right) + \hat{d}\,\rho\,\text{Int}\left(\frac{x_i'}{\rho}\right)\right) - \text{sgn}(x'(T))\,\hat{\mu} \tag{12}$$

Here the following dimensionless multiplier appears

$$\rho = \frac{r_{\text{in}}}{r_{\text{out}}\,\tau^2}.$$

Using the above notations, the *micro-chaos map* can be written as:

$$\mathbf{y}_{i+1} = \mathbf{U}\,\mathbf{y}_i + \mathbf{B}\,(\text{Int}(\mathbf{K}\,\rho\,\text{Int}(\mathbf{y}_i/\rho)) + \text{sgn}(y_{i,2})\,\hat{\mu})\,. \tag{13}$$

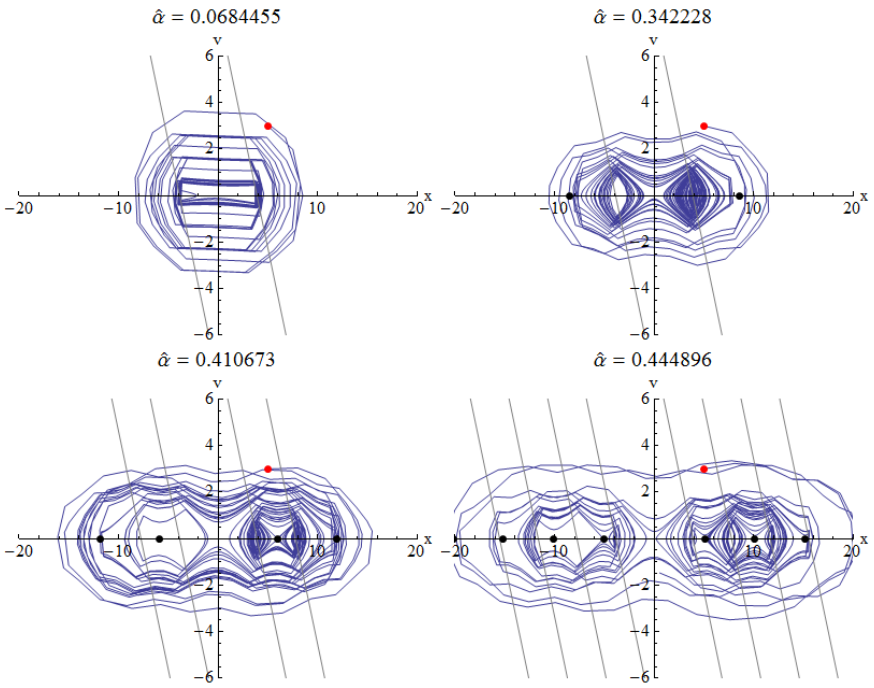

Figure 2: Example attractors of Map (11). $\hat{\beta} = 8.25049 \times 10^{-3}$, $\hat{p} = 0.2576$, $\hat{d} = 0.1256$, $\hat{\mu} = 0$.

Simulations and Topological pattern

Consider the case, when rounding is applied to the output (Map (11)). The unstable fixed points of the map lie on the x-axis:

$$\mathrm{Int}(\hat{p}\, x_u) = \hat{\alpha}^2\, x_u \rightarrow x_u = \frac{k}{\hat{\alpha}^2}, \qquad k \in \mathbb{Z}. \tag{14}$$

The equation of switching lines

$$\mathrm{Int}(\hat{p}\, x + \hat{d}\, v) \rightarrow v = \frac{l - \hat{p}\, x}{\hat{d}}, \qquad l \in \mathbb{Z}\backslash\{0\}. \tag{15}$$

The dynamics of the system between two switching lines is unstable, therefore *stable* equilibria (i.e. attractors) are expected to be on the switching lines. The intersections between the switching lines and the x axis are:

$$x_s = \frac{l}{\hat{p}}, \qquad l \in \mathbb{Z}\backslash\{0\}. \tag{16}$$

Based on topological assumptions, unstable fixed points and attractors should occur alternately. Restricting control parameters to the stable domain, ($\hat{p} > \hat{\alpha}^2$), the index of the last fixed point (and also the index of the last attractor) can be expressed as

$$l_{\max} = \mathrm{Int}\left(\frac{\hat{p}}{\hat{p} - \hat{\alpha}^2}\right). \tag{17}$$

Therefore an estimation of upper limit of control error could be given for the case, when the eigenvalues of $\mathbf{U}$ are positive and real. (Necessary conditions for this estimation are currently being elaborated.)

$$x_{\max} = \frac{1}{\hat{p} - \hat{\alpha}^2}. \tag{18}$$

Attractors can be small enough to maintain their own basin of attraction, however they could also behave as repellors, when two or more of them make a larger attractor, reaching over several switching lines. This case is illustrated in Fig. 2.

Cell mapping results

Cell mapping (CM) methods are tools for the global investigation of the long term behaviour of nonlinear dynamical systems [4]. Using CM methods, periodic and chaotic solutions of the equations of motion can be found, moreover the basin of attraction can also be determined. Simple cell mapping (SCM) method was applied to (11), to determine whether the chaotic attractors disappear due to the friction. Results show, that the chaotic behaviour remains, and the previously unstable fixed points are becoming attractors. Consider Figure 3. showing the basin of attraction (coloured bands) of

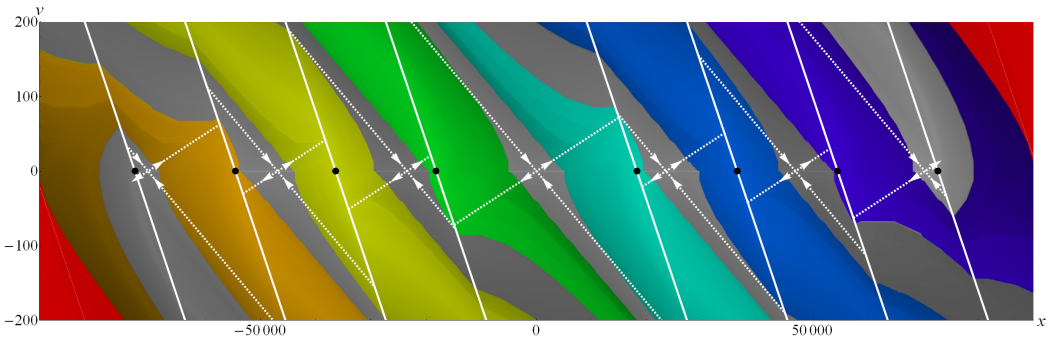

Figure 3: SCM results for $\hat{\alpha} = 6.53 \times 10^{-3}$, $\hat{\beta} = 2.0 \times 10^{-3}$, $\hat{p} = 5.5 \times 10^{-5}$, $\hat{d} = 2.5 \times 10^{-3}$, $\mu_0 = 0.2$

chaotic attractors (black dots), switching lines (white), stable and unstable manifolds of fixed points (white, dashed). Cell mapping results encouraged us to carry out measurements on a real PD-controlled inverted pendulum.

Measurements

Measurement setup

Measurements were carried out using a simple inverted pendulum (made of an aluminium rod and a weight) attached to a DC-motor (Maxon RE-max 32). The pendulum is attached directly to the shaft of the motor, it has a rotary encoder for angular position measurement. The setup is controlled with a PIC microcontroller (PIC24FJ128GA010) which calculates the angular velocity as the derivative of the position and calculates the control effort. The motor is driven through an H-bridge which enables it to run in both directions. (See Figure 4.)

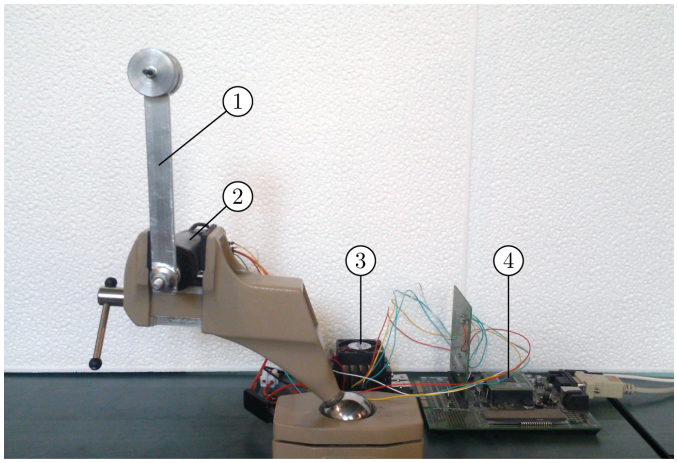

Figure 4: The measurement setup. 1: inverted pendulum, 2: DC-motor, 3: H-bridge, 4: PIC microcontroller.

System parameters

The rotary encoder attached to the motor shaft counts 2000 per revolutions, therefore the resolution of the measured position is:

$$r_{\text{in}} = \frac{2\pi}{2000} = 0.00314159\,[\text{rad}] \tag{19}$$

The nominal voltage of the DC motor is $U_0 = 12\,[\text{V}]$, the motor resistance is $R_m = 2.5\,[\Omega]$ and the motor constant is $K_m = 24.3 \times 10^{-3}\,[\frac{\text{Nm}}{\text{A}}]$ (See [6]). The microcontroller drives the motor by means of PWM and the full range of duty cycle is divided into $r_{\text{PWM}} = 794$ units (where 794 corresponds to 100% duty cycle). Therefore the resolution of the control torque:

$$r_{\text{out,min}} = \frac{K_m\, U_0}{R_m\, r_{\text{PWM}}} = 0.000146902\,[\text{Nm}] \tag{20}$$

This resolution can be made more coarse by rounding r_{PWM} on the microcontroller. Its maximum value for the device is:

$$r_{\text{out,max}} = \frac{K_m\, U_0}{R_m\, 1} = 0.11664\,[\text{Nm}] \tag{21}$$

The logarithmic decrement was measured to find the damping ratio of the system. With $\delta = 0.762943$ and $T = 0.71\,[\text{s}]$ the damping ratio

$$\zeta = \frac{1}{\sqrt{1 + (\frac{2\pi}{\delta})^2}} = 0.120541 \tag{22}$$

and the damped and undamped natural frequencies are

$$\omega_d = \frac{2\pi}{T} = 8.84956\,\left[\frac{\text{rad}}{\text{s}}\right], \qquad \alpha = \frac{\omega_d}{\sqrt{1-\delta^2}} = 13.6891\,\left[\frac{\text{rad}}{\text{s}}\right]. \tag{23}$$

The sampling time of the controller is $\tau = 0.005\,[\text{s}]$, consequently the dimensionless parameters are:

$$\hat{\alpha} = \alpha\tau = 6.84457 \times 10^{-2}, \qquad \hat{\beta} = \zeta\alpha\tau = 8.25049 \times 10^{-3}. \tag{24}$$

Therefore, the value of the dimensionless multiplier is in the range:

$$\rho = \frac{r_{\text{in}}}{r_{\text{out}}\,\tau^2} = 1077 \ldots 855425.$$

Results

Measurements were carried out with various control parameters at $\rho = 3719$ and $\hat{\mu} = 157$. Time series analysis was carried out on the results using the TISEAN package [5]. Unfortunately, the results of time series analysis did not verify chaotic behaviour explicitly. The fitted line shows power law connection. (See Fig. 6)

Conclusions

An experimental device with variable control effort resolution (r_{out}) and variable input resolution (r_{in}) was used to show the existence of micro-chaotic behaviour. Measurements generally agree with simulation results, however, time series analysis could not prove the chaotic behaviour. This could be the result of non-negligible processing delay in the measurement device. Further analysis of the measured data sets is in progress.

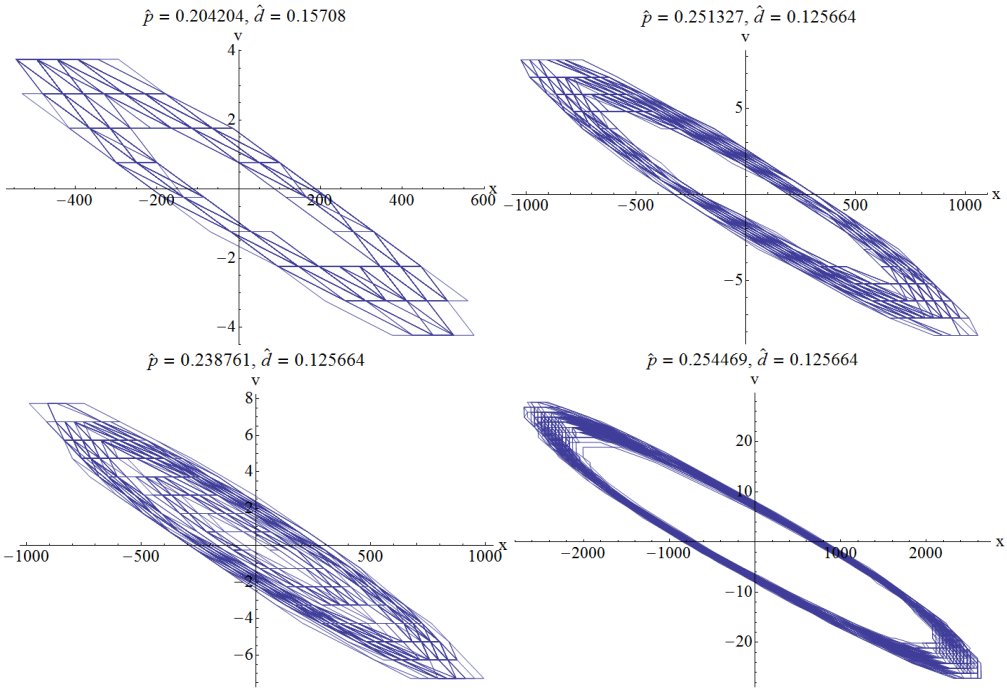

Figure 5: Measured data sets with $\rho = 3719$, $\hat{\mu} = 157$

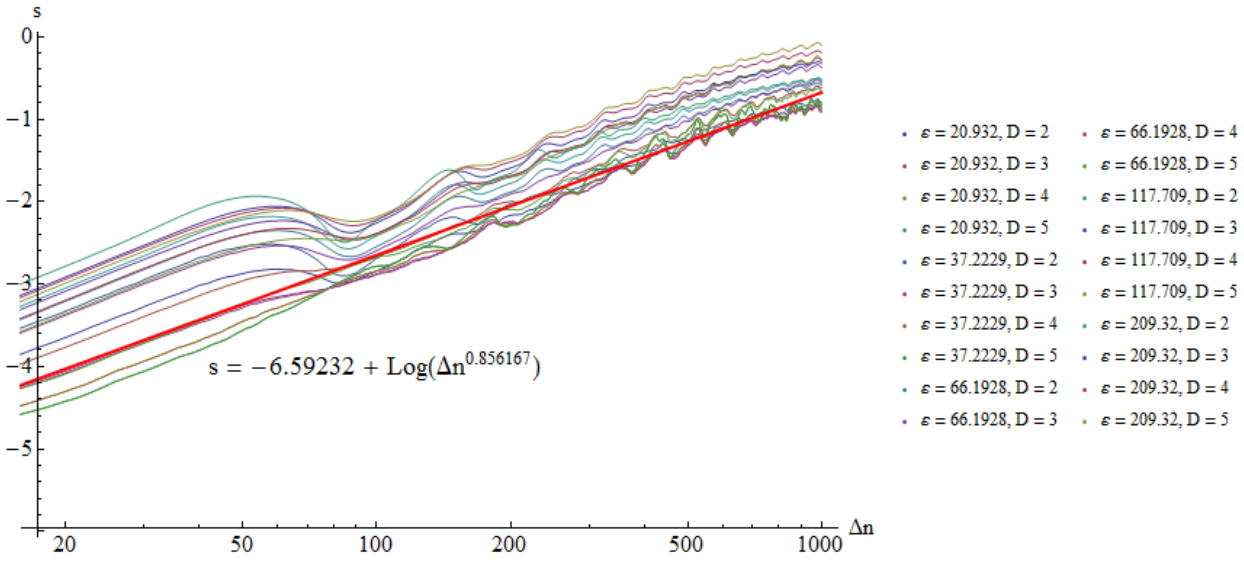

Figure 6: Results of the time series analysis, s is the stretching factor, Δn is the number of steps.

Acknowledgements

This research was supported by the Hungarian National Science Foundation under grant no. OTKA K 83890.

References

[1] G. Csernák, G. Stépán (2010) Digital Control as Source of Chaotic Behavior. *International Journal of Bifurcation and Chaos* **20(5)**: pp. 1365-1378

[2] G. Csernák, G. Stépán (2011) Sampling and Round-off, as Sources of Chaos in PD-controlled Systems. *Proceedings of the 19th Mediterranean Conference on Control and Automation*

[3] G. Csernák, G. Stépán (2012) Disconnected Chaotic Attractors in Digitally Controlled Linear Systems, *Proceedings of the 8th WSEAS International Conference on Dynamical Systems and Control, ISBN: 978-1-61804-103-6*: pp. 97-102

[4] J. A. W. van der Spek (1994) Cell Mapping Methods: Modifications and Extensions. *PhD Thesis*, Eindhoven University of Technology, Eindhoven

[5] R. Hegger, H. Kantz, T. Schreiber (1999) Practical implementation of nonlinear time series methods: The TISEAN package, *CHAOS* **9**: pp. 413

[6] Cs. Budai, L. L. Kovács (2013) Limitations Caused by Sampling and Quantization in Position Control of a Single Axis Robot. *OWD 2013, XV International PhD Workshop, Gliwice, Poland, ISBN: 978-83-935427-2-7*: pp. 466-471